Theoretical investigation of electron-impact multiple ionization of O II-IV ions

Yulong Ma,[1] Ling Liu,[1,*] Yong Wu,[1,2,†] Yizhi Qu,[3] and Jianguo Wang[1]

[1]*Key Laboratory of Computational Physics, Institute of Applied Physics and Computational Mathematics, 100088 Beijing, China*

[2]*HEDPS, Center for Applied Physics and Technology, Peking University, 100084 Beijing, China*

[3]*School of Optoelectronics, University of Chinese Academy of Sciences, 100049 Beijing, China*

(Received 1 January 2020; accepted 28 April 2020; published 20 May 2020)

The electron-impact double ionization (DI) and triple ionization (TI) for O II-IV ions are investigated using multistep approaches within the framework of many-body perturbation theory. The indirect DI and TI are treated as the single ionization of an inner-shell 1*s* electron followed by the single and double Auger decays, respectively. The knockout mechanism is employed to deal with the direct ionization process. The present approaches reproduce the available experimental cross sections for the DI of O II-IV ions with much better accuracy compared to previous calculations. The TI cross sections of the O II ion are calculated, which are in good agreement with the recent experimental data [Lecointre *et al.*, J. Phys. B **46**, 205201 (2013)]. It is found that the electron correlation effect and the energy distribution of the intermediate electron, which is taken as the incident electron of the subsequent knockout process, play an important role in the multistep treatment of the multiple ionization process.

DOI: 10.1103/PhysRevA.101.052703

I. INTRODUCTION

The electron-impact multiple ionization (MI), which leads to the ionization of many electrons of an atomic system, is attracting considerable interest since investigations of such processes could give important information on the many-body correlation effect in the dynamics of electron-ion collisions [1,2] and charge state distribution (CSD). Accurate CSD data are needed to determine and model physical properties such as thermal structure and line emission of laboratory and astrophysical plasmas [3–5].

Over several decades, a large number of experimental studies on the MI have been carried out, as reviewed in Refs. [5–7]. For example, by applying the animated crossed beam method, the MI cross sections of various ionization stages of carbon, nitrogen, and oxygen elements have been measured [8–10]. On the other hand, theoretical investigations of the MI are very challenging due to the complex nature of the many-body correlation that involves at least three continuum electrons moving in the ionic field. Thus, a few theoretical efforts have been made and focused mainly on the electron-impact double ionization (DI), that is the simplest and the most fundamental MI process. For example, the nonperturbative time-dependent close-coupling (TDCC) method [11–13] can reproduce well the DI cross sections for helium [11]. However, as the number of coupled channels increases rapidly due to the coupling of three active electrons for complex systems [13], the large amount of computation of the TDCC could challenge the current computational capacity. Alternatively, in the perturbative approximations, two different and competing processes of the direct and indirect MI are distinguished [14]. The electron-impact indirect double ionization (IDI) can be generally described as a two-step process, in which a primary electron-impact single ionization (SI) of an inner-shell electron is followed by a single Auger (SA) decay [14]. The electron-impact direct double ionization (DDI) has been considered in terms of the shakeoff (SO) [15] and two-step (TS) [16] mechanisms. In the SO mechanism the incident electron collides with the target and removes quickly a primary bound electron. This causes a sudden change in the atomic field so that the secondary electron may relax to an unbound state of the remaining ion. When the incident electron collides with the target, the primary SI can proceed and leads to a remaining ion as well as "intermediate" scattered and ejected electrons. Subsequently, such an intermediate ejected electron and scattered electron knock out another bound electron of the remaining ion, which are referred to as the TS1 and TS2 mechanisms, respectively.

Recently, Jonauskas and coworkers [17–20] presented the DDI as a sequence of the ionization-ionization, excitation-ionization-ionization, and ionization-excitation-ionization processes. In their approaches, the energy of an intermediate electron has to be analyzed to remove the disagreement between theoretical results and the experimental data. Specifically, in the case of low incident energies, all the excess energy after the primary SI is taken by the intermediate electron. For the intermediate-high incident energies, the excess energy is shared between the intermediate electrons. The former and latter cases are denoted as Jonauskas *et al.* (I) and Jonauskas *et al.* (II), respectively, in the following text and figures for comparing conveniently. Although significant efforts were devoted to the analyses of the energy of the intermediate electron, some obvious differences between their theoretical results and the experimental cross sections remain for the DI of O^+, O^{2+}, and O^{3+} ions [17]. Therefore, further theoretical studies are required to especially explore the role

*liu_ling@iapcm.ac.cn

†wu_yong@iapcm.ac.cn

of the energy distribution of the intermediate electron in the multistep approach for obtaining the DI cross sections with satisfactory accuracy.

Later, based on the knockout (KO) and SO mechanisms that have been applied successfully to deal with the double ionization by absorption of one [21,22] or two [23] photons, the multiple-Auger decay [24–29], and the double-*K*-vacancy production in ion-atom collisions [30,31], Liu *et al.* [32] employed corresponding approximate formulas to calculate the DDI cross section of C^+, N^+, and O^+ ions. Their results agree reasonably with the available experimental data and illustrate that the KO mechanism is dominant, which indicates the validity of the KO mechanism for describing the DDI process.

Apart from the DI of O^+, O^{2+}, and O^{3+} ions mentioned above, the cross sections for the electron-impact triple ionization (TI) of the O^+ ion have been measured by the animated crossed beam method [9,10]. To the best of our knowledge, no *ab initio* studies on such a complex process involving five particles of a final ion and four outgoing continuum electrons are available. Therefore, theoretical studies on the TI of the O^+ ion are highly expected.

In the present paper, we apply the multistep approach to investigate the DI and TI including the direct and indirect processes for O^+, O^{2+}, and O^{3+} ions. The IDI and electron-impact indirect triple ionization (ITI) are described as the primary single ionization of an inner-shell $1s$ electron followed by the SA and the double Auger (DA) decays, respectively. In our previous works [26–29], the KO and SO mechanisms derived from the many-body perturbation theory (MBPT) [24] are employed to obtain the direct multiple-Auger rates. Here, we extend straightforwardly the KO mechanism to describe the DDI and the electron-impact direct triple ionization (DTI). We carry out large-scale configuration-interaction (CI) calculations for the DI cross sections of O^+, O^{2+}, and O^{3+} ions using the flexible atomic code (FAC) with the distorted-wave (DW) approximation [33]. Furthermore, the *ab initio* TI cross sections of the O^+ ion are also calculated. Another purpose of the present paper is to illustrate the role of the energy distribution of the intermediate electron in the multistep approach for describing the multiple ionization process.

The remainder of the paper is structured as follows. Section II describes the theoretical approach for calculating the DI and TI cross sections. In Sec. III the calculated cross sections are compared with the available theoretical and experimental data, and the corresponding discussions are given. In Sec. IV the conclusions are given.

II. THEORETICAL METHOD

In the MI, as mentioned above, the ionization of the electrons in a target ion can proceed either via a direct process or via an indirect process involving autoionization of an intermediate state [14]. Thus, the total MI cross section is obtained by the sum of contributions from these two processes.

A. Electron-impact double-ionization cross section

In this paper, we use the KO mechanism [21,22,24–30] to deal with the DDI. It is noted that the contributions from the SO mechanism are neglected for the following reasons. First, it is well known that the SO mechanism is weak for the low and intermediate energies [32,34]. Second, at high energies, since the contributions from the indirect process become dominant to the total DI cross section in the present cases of O^+, O^{2+}, and O^{3+} ions, although the SO mechanism might be important to the DDI, it still has a negligible impact on the total cross section.

The KO mechanism describes the correlated dynamics of the two electrons: an intermediate electron knocks out another electron in an $(e, 2e)$-like process [21]. Based on the KO mechanism, our two-step approach decomposes the DDI into the primary SI and the subsequent KO (electron-electron inelastic scattering) process:

$$e^- + O^{n+} \xrightarrow{\text{SI}} O^{(n+1)+} + 2e^- \xrightarrow{\text{KO}} O^{(n+2)+} + 3e^-, \quad (1)$$

where $n = 1$, 2, and 3 represent the O^+, O^{2+}, and O^{3+} ions, respectively. In the present two-step approach, any one of the intermediate electrons in the primary SI is treated as the incident electron of the subsequent KO process. Then the DDI cross section with the incident electron energy ε_0 can be obtained by

$$\sigma_{if}^{\text{DDI}}(\varepsilon_0) = \sum_m \sigma_{im}^{\text{SI}}(\varepsilon_0) \int_{E_{fm}}^{\varepsilon_0 - E_{mi}} \rho_{im}^{\text{SI}}(\varepsilon_0, \varepsilon_m) \Omega_{mf}^{\text{KO}}(\varepsilon_m) d\varepsilon_m, \quad (2)$$

where $\sigma_{im}^{\text{SI}}(\varepsilon_0)$ is the cross section of the primary SI from the initial ionic state O^{n+} (with energy E_i) to the intermediate ionic state $O^{(n+1)+}$ (with energy E_m) with two intermediate electrons sharing the excess energy of $\varepsilon_0 - E_{mi}$, where $E_{mi} = E_m - E_i$. ε_m is the kinetic energy of the intermediate electron. It is noted that any one of the intermediate electrons will participate in the subsequent KO process with the collision strength $\Omega_{mf}^{\text{KO}}(\varepsilon_m)$. In our treatment of KO, the intermediate electrons are indistinguishable, and thus we assume that one of the intermediate electrons takes the energy ranging from zero to $\varepsilon_0 - E_{mi}$. Hence the contributions of all intermediate electrons can be included by integrating over the energy from $E_{fm} = E_f - E_m$ (E_f is the energy of the final ionic state $O^{(n+2)+}$) to $\varepsilon_0 - E_{mi}$ in Eq. (2) since the intermediate electron with the energy $0 \leqslant \varepsilon_m < E_{fm}$ is energetically forbidden to ionize a bound electron of the intermediate ion, while $\varepsilon_m = \varepsilon_0 - E_{mi}$ means that the intermediate electron takes all the excess energy of the primary SI. It is noted that the two intermediate electrons are indistinguishable (we do not talk of the ejected and the scattered electron of the primary SI), but the present approach clearly includes the contributions from both the TS1 and the TS2 processes mentioned in Sec. I according to Eqs. (1) and (2).

As ε_m distributes continuously, the energy distribution $\rho_{im}^{\text{SI}}(\varepsilon_0, \varepsilon_m)$ is introduced in Eq. (2), and it should be normalized to unity on the energy scale, $\int_0^{\varepsilon_0 - E_{mi}} \rho_{im}^{\text{SI}}(\varepsilon_0, \varepsilon_m) d\varepsilon_m = 1$. In the present approach, the energy distribution could be simulated with using the normalized differential cross section (DCS), $d\tilde{\sigma}^{\text{SI}}(\varepsilon_0, \varepsilon)/d\varepsilon$, of the primary SI according to

$$\rho^{\text{SI}}(\varepsilon_0, \varepsilon) = \frac{d\tilde{\sigma}^{\text{SI}}(\varepsilon_0, \varepsilon)}{d\varepsilon} = \frac{1}{N} \frac{d\sigma^{\text{SI}}(\varepsilon_0, \varepsilon)}{d\varepsilon}, \quad (3)$$

where normalization factor $N = \int_0^E \frac{d\sigma^{\rm SI}(\varepsilon_0,\varepsilon)}{d\varepsilon} d\varepsilon$ and E is the excess energy of the SI. In the present paper, the DCS $d\sigma^{\rm SI}(\varepsilon_0,\varepsilon)/d\varepsilon$ is obtained by the analytic formula (44) in Ref. [35], based on the binary-encounter-dipole (BED) model.

It is worth pointing out that (a) the energy distribution is particularly introduced and stressed in the present approach for illuminating how the intermediate electron contributes to the two-step treatment of the DDI; (b) such energy distribution can be determined by using the DCS of the primary SI [see Eq. (3)]; and (c) the analytic BED formula [35] is employed to simplify the calculations of the energy distribution. It is noted that one can obtain directly the DDI cross sections by using the DCS from *ab initio* calculations since both of the cross sections $\sigma^{\rm SI}(\varepsilon_0)$ and energy distributions $\rho^{\rm SI}(\varepsilon_0,\varepsilon_m)$ can be determined in terms of the DCS.

For light oxygen ions, the IDI process can be generally described as the primary SI of an inner-shell $1s$ electron with the SA decay [14]:

$$e^- + {\rm O}^{n+} \xrightarrow{\rm SI} {\rm O}^{(n+1)+}(1s^{-1}) + 2e^- \xrightarrow{\rm SA} {\rm O}^{(n+2)+} + 3e^-, \quad (4)$$

which is denoted as the SI-SA process. Thus, the SI-SA cross section can be obtained by

$$\sigma_{if}^{\rm IDI}(\varepsilon_0) = \sum_m \sigma_{im}^{\rm SI}(\varepsilon_0) B_{mf}^{\rm SA}, \quad (5)$$

where $\sigma_{im}^{\rm SI}(\varepsilon_0)$ is the SI cross section from the initial state to an intermediate autoionizing state ${\rm O}^{(n+1)+}(1s^{-1})$ which undergoes the SA with the branching ratio (BR) of $B_{mf}^{\rm SA}$:

$$B_{mf}^{\rm SA} = \frac{A_{mf}^{\rm SA}}{\sum_f A_{mf}^{\rm SA} + \sum_s A_{ms}^r}. \quad (6)$$

Here, A_{ms}^r and $A_{mf}^{\rm SA}$ are the radiative and SA rates for the intermediate autoionizing state ${\rm O}^{(n+1)+}(1s^{-1})$, respectively. In Eq. (6), the DA rates are neglected as they are about two orders of magnitude less than the SA rates [36].

B. Electron-impact triple-ionization cross section

In the DTI, the incident electron collides with the O^+ ion and removes three bound electrons simultaneously. The KO mechanism is employed to describe such a process by including the important final-state correlation after the primary DDI, while the weak SO mechanism is neglected due to its negligible contribution to the total cross section. Then the DTI of the O^+ ion is treated as a combination of the primary DDI and the subsequent KO process:

$$e^- + {\rm O}^+ \xrightarrow{\rm DDI} {\rm O}^{3+} + 3e^- \xrightarrow{\rm KO} {\rm O}^{4+} + 4e^-. \quad (7)$$

The corresponding DTI cross section is then given by

$$\sigma_{if}^{\rm DTI}(\varepsilon_0) = \sum_m \sigma_{im}^{\rm DDI}(\varepsilon_0) \int_{E_{mf}}^{\varepsilon_0 - E_{mi}} \rho_{im}^{\rm DDI}(\varepsilon_0,\varepsilon_m) \Omega_{mf}^{\rm KO}(\varepsilon_m) d\varepsilon_m. \quad (8)$$

Here, $\sigma_{im}^{\rm DDI}(\varepsilon_0)$ is the primary DDI cross section [given in Eq. (2)] with the incident electron energy ε_0; $\Omega_{mf}^{\rm KO}(\varepsilon_m)$ is the collision strength of the KO that ionizes a bound electron of the intermediate O^{3+} ion by the intermediate electrons with the energy ε_m; $E_{mi} = E_m - E_i$ and $E_{fm} = E_f - E_m$, where E_i, E_m, and E_f are the energy of the ionic states of O^+, O^{3+}, and O^{4+}, respectively. In Eq. (8) it is assumed that one of the intermediate electrons takes the energy ranging from zero to $\varepsilon_0 - E_{mi}$. According to the works [32,37,38], the energy of the ejected electron distributes continuously in the DDI. Hence the normalized energy distribution $\rho_{im}^{\rm DDI}(\varepsilon_0,\varepsilon_m)$ of the intermediate electron is also introduced, which can be simulated by using the DCS of the primary DDI.

In our simple approaches, the ionization of electrons in the DDI results mainly from final-state correlations of the electron-electron interaction with the KO mechanism. Hence the differential collision strength with respect to the individual energy, $d\Omega_{mf}^{\rm KO}(\varepsilon_m,\varepsilon)/d\varepsilon$, is employed. Here, ε is the kinetic energy of the ejected electron in the KO process, and we safely assume that such energy could serve approximately as the energy of one of the outgoing continuum electrons in the DDI. Then, to obtain the normalized energy distribution of the DDI, $\rho^{\rm DDI}(\varepsilon_0,\varepsilon)$, Eq. (2) of the DDI cross section is rewritten straightforwardly as

$$\begin{aligned}\rho^{\rm DDI}(\varepsilon_0,\varepsilon) &= \frac{d\tilde{\sigma}^{\rm DDI}(\varepsilon_0,\varepsilon)}{d\varepsilon} \\ &= \sum_m \sigma_{im}^{\rm SI}(\varepsilon_0) \int_{E_{fm}}^{\varepsilon_0 - E_{mi}} \rho_{im}^{\rm SI}(\varepsilon_0,\varepsilon_m) \\ &\quad \times \frac{d\tilde{\Omega}_{mf}^{\rm KO}(\varepsilon_m,\varepsilon)}{d\varepsilon} d\varepsilon_m, \end{aligned} \quad (9)$$

where $d\tilde{\sigma}^{\rm DDI}(\varepsilon_0,\varepsilon)/d\varepsilon$ and $d\tilde{\Omega}_{mf}^{\rm KO}(\varepsilon_m,\varepsilon)/d\varepsilon$ are the normalized DCS of the primary DDI and collision strength of the KO, respectively. Since the present approach treats the KO simply as an electron-impact ionization, the $d\tilde{\Omega}_{mf}^{\rm KO}(\varepsilon_m,\varepsilon)/d\varepsilon$ can be also obtained approximately by the BED model [35]. As an independent check, it is shown in Fig. 1 that the present energy distributions are in reasonably good agreement with the experimental values [38] (the maximal magnitude is normalized to 1 for comparison) of the ejected electrons in the DDI of argon at the incident energy of 123 eV. This indicates the validity of the present approaches for evaluating the energy distribution of the ejected electron in the DDI. It is noted that as the states from the configurations $3s^2 3p^4$ (the continuum electrons with energy range zero to ≈80 eV) and $3s3p^5$ (the continuum electrons with energy range zero to ≈65 eV) in final Ar^{2+} are taken into account a slightly nonsymmetric U-shaped energy distribution is observed in Fig. 1.

In the ITI of the O^+ ion, electrons could be ejected in a stepwise manner through the creation and decay of intermediate autoionizing states, which can be mainly considered in the following two categories:

$$e^- + {\rm O}^+ \xrightarrow{\rm DI} {\rm O}^{*3+} + 3e^- \xrightarrow{\rm SA} {\rm O}^{4+} + 4e^-, \quad (10)$$

$$e^- + {\rm O}^+ \xrightarrow{\rm SI} {\rm O}^{2+}(1s^{-1}) + 2e^- \xrightarrow{\rm DA} {\rm O}^{4+} + 4e^-. \quad (11)$$

In Eq. (10), the intermediate autoionizing states O^{*3+} that lie above the O^{4+} threshold are created by the primary DI of the O^+ ion. Then these intermediate states can decay further to the O^{4+} states via the SA decay. However, from

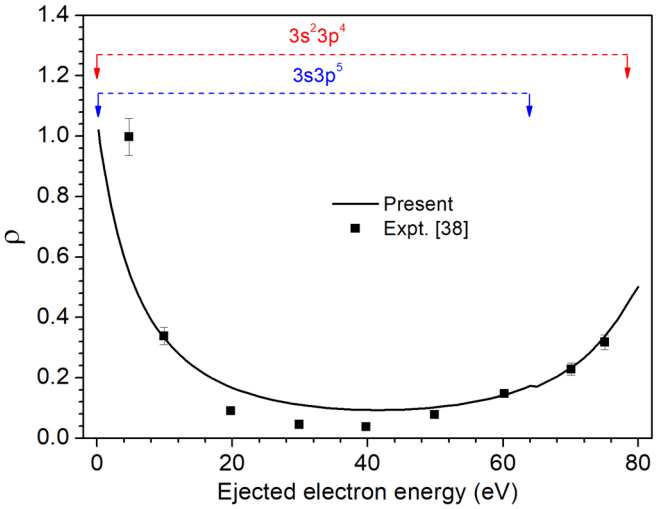

FIG. 1. Comparison of the energy distribution (the maximal magnitude is normalized to 1.0) between the present results and the experimental data for the ejected electrons of the electron-impact direct double ionization of argon at the incident energy of 123 eV. The contributions from states of $3s^2 3p^4$ and $3s3p^5$ in the final Ar^{2+} ion are included with excess energy ranging from 0 to ≈80 eV and 0 to ≈65 eV, respectively.

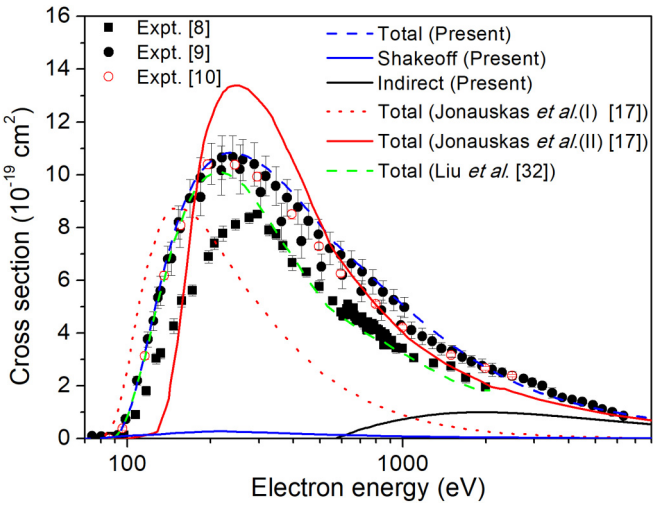

FIG. 2. Theoretical and experimental cross sections for the electron-impact double ionization of the O^+ ion. Total: including the cross sections of the direct and indirect processes. Indirect: cross section of the indirect process. Shakeoff: cross section from the shakeoff mechanism.

our test calculations the cross sections of the DI of the O^+ ion leading to such states O^{*3+} are estimated roughly to be at most $\sim 10^{-23}$ cm^2 much smaller than the experimental results ($\sim 10^{-20}$ cm^2) [9,10]. Hence the contributions of the channel (10) are neglected in our calculations.

Therefore, in the present paper we concentrate on the most important channel (11): a primary SI of the inner-shell $1s$ electron followed by the DA decay, which is referred to as the SI-DA process. Then the corresponding cross section can be obtained with

$$\sigma_{if}^{\mathrm{ITI}}(\varepsilon_0) = \sum_m \sigma_{im}^{\mathrm{SI}}(\varepsilon_0) B_{mf}^{\mathrm{DA}}, \tag{12}$$

where $\sigma_{im}^{\mathrm{SI}}(\varepsilon_0)$ is the SI cross section from the initial states to intermediate autoionizing states O^{2+} $(1s^{-1})$ that undergo the DA decay with the BR of B_{mf}^{DA}:

$$B_{mf}^{\mathrm{DA}} = \frac{A_{mf}^{\mathrm{DA}}}{\sum_f A_{mf}^{\mathrm{DA}} + \sum_k A_{mk}^{\mathrm{SA}} + \sum_s A_{ms}^{r}}, \tag{13}$$

where A_{mf}^{DA} is the DA rate of the intermediate autoionizing state O^{2+} $(1s^{-1})$.

The FAC package [33] is employed to obtain the SI cross section and the collision strength of the KO mechanism as well as the radiative and single Auger rates, which implements the Dirac-Fock-Slater approach and the DW approximation for the continuum electron. The DA rates are calculated based on the SO and KO mechanisms (for details please refer to our previous papers [26–28]).

III. RESULTS AND DISCUSSION

As many-electron correlation effects lead dominantly to the MI, the electron correlation effect could play an essential role in the accurate calculations of the MI cross sections. Furthermore, taking the O^+ ion as an example, the cross-section calculations concern three different successive ionization stages, i.e., O^+, O^{2+}, and O^{3+} ions for the DDI as well as four different successive O^+ to O^{4+} ions for the DTI, according to our approximate formulas (2) and (8), respectively. Thus, one should consider the balance of the electron correlation for the ions with different ionization stages when using the standard CI procedure. In our CI approximation implemented by the FAC package [33], the main configurations produced by single and double excitations from the respective ground configurations of O^+, O^{2+}, O^{3+}, O^{4+}, and O^{5+} ions to the orbitals of $2p$, $3l$ ($l = s$, p, and d) and $4l'$ ($l' = s$, p, d, and f) are considered for including the electron correlations on the same footing. For example, for the O^+ ion the interactions among the following configurations are included: $2s^2 2p^3$, $2s2p^4$, $2p^5$, $[2s, 2p]^4 nl$, and $[2s, 2p]^3 nln'l'$ ($nl, n'l' = 3s, 3p, 3d, 4s, 4p, 4d$, and $4f$), where $[2s, 2p]^m$ indicates that m electrons are distributed between the $2s$ and $2p$ orbitals. In order to generate bound and continuum orbitals, the central potential constructed by the ground configuration of the intermediate ion is adopted for the DDI of O^+, O^{2+}, and O^{3+} ions; moreover, the ground configuration of the intermediate O^{2+} ion for the primary DDI and the ground configuration of the intermediate O^{3+} for the subsequent KO, respectively, are adopted for the DTI of O^+.

A. Electron-impact double ionization

The present cross sections for the DI of the O^+ ion are compared with the available theoretical [17,32] and experimental [8–10] data in Fig. 2. The present double-ionization threshold of 88.53 eV is in reasonable agreement with the NIST [39] value of 90.06 eV. In Fig. 2, the latest experimental data of Westermann *et al.* [9] and Lecointre *et al.* [10] are nearly consistent with each other, while they are about 35% greater than the earlier experimental values of Zambra *et al.* [8]. It

is found that present cross sections agree well with the latest experimental data [9,10] over the entire energy up to about 6000 eV.

The contribution from the SO mechanism is also displayed in Fig. 2. It is found that the SO mechanism has a rather small contribution to the DDI cross section at energies less than 575 eV where the total cross section results from only the direct process. Moreover, at high energies such as greater than about 5000 eV, the cross section from the indirect process is larger than that from the direct channel and becomes dominant. Therefore, as assumed in Sec. II A, it is quite reasonable to neglect the contributions from the SO mechanism for the entire energy range investigated, which is also supported by the work of Liu *et al.* [32]. Since they used the KO mechanism that is conceptually similar to the present one, the present DI cross sections of the O^+ ion are quite consistent with their calculations [32] near the threshold, as shown in Fig. 2. However, their results decrease rapidly with increasing energy and become smaller than both of the present results and the latest experimental data [9,10] at incident energies greater than about 200 eV. This difference might result from the choice of the potentials used to generate the continuum orbitals, because it could affect the calculations of the DDI cross section [40], especially for the low-Z ions.

As illustrated by Jonauskas *et al.* [17], due to the absence of proper energy distributions of the intermediate electron, they had to perform two different calculations which are denoted as Jonauskas *et al.* (I) and (II) for the low and intermediate-high incident energies, respectively. However, some obvious differences between the calculations and the experimental data are still found, as shown in Fig. 2. For instance, the results of Jonauskas *et al.* (II) overestimate the experimental measurements [8–10] at intermediate energies ranging from 150 to 600 eV and are significantly inconsistent with the energy dependence of the cross section.

It is found from Fig. 2 that the present two-step approach based on the KO mechanism reproduces quite well the latest experimental measurements [9,10] for the DI of the O^+ ion. We think the considerable improvements over the previous work of Jonauskas *et al.* [17] are mainly attributed to the suitable energy distributions [see Eqs. (2) and (3)] of the intermediate electron employed in the present approach. Furthermore, this indicates the validity of the BED model [35] for simulating the energy distribution of the ejected electron in the primary SI. A similar model has been also employed successfully to obtain the energy distributions of Auger electrons in the direct DA of Ne^+ $1s^{-1}$ [27].

To obtain more insight into the energy behavior of intermediate electrons, taking the primary SI $e^- + O^+(1s^2 2s^2 2p^3\,{}^4S) \rightarrow O^{2+}(1s^2 2s^2 2p^2\,{}^3P) + 2e^-$ in the DDI of the O^+ ion as an example, the energy distributions of the intermediate electrons are plotted in Fig. 3. In this figure, the maxima of the magnitudes of energy distribution and intermediate-electron energy are normalized to be 1 in the y and x axis, respectively. For example, the value of 1 in the x axis means that the intermediate electron takes all the excess energy of the primary SI. It is noted in Fig. 3 that the intermediate electron with solid-line energy distribution contributes to the DDI cross section because only such an electron in this energy range is energetically sufficient to knock out a secondary bound electron of the intermediate O^{2+} ion in the subsequent KO process. As shown in Fig. 3, in the case of the low incident electron energy of 95 eV, the intermediate electron taking almost all the excess energy will contribute mainly to the DDI cross section. This is consistent with the case of Jonauskas *et al.* (I) [17] for the low incident energy. For high incident energy such as 2000 eV, our results indicate that the intermediate electron with low and high energies has a significant contribution to the cross section. However, this differs noticeably from the case of Jonauskas *et al.* (II) in which the intermediate electron tends to equally share the excess energy [17]. It is worth noting that we actually obtain the DDI cross section by averaging the contributions of the intermediate electron weighted with the corresponding energy distribution, as expressed in Eq. (2). Therefore, to some extent, one can obtain the proper DDI cross section by choosing a proper energy of the intermediate electron in the two-step approach, as proposed by Jonauskas and coworkers [17–20]. However, the present approach can provide the DI cross sections, which are in a good agreement with the experimental data.

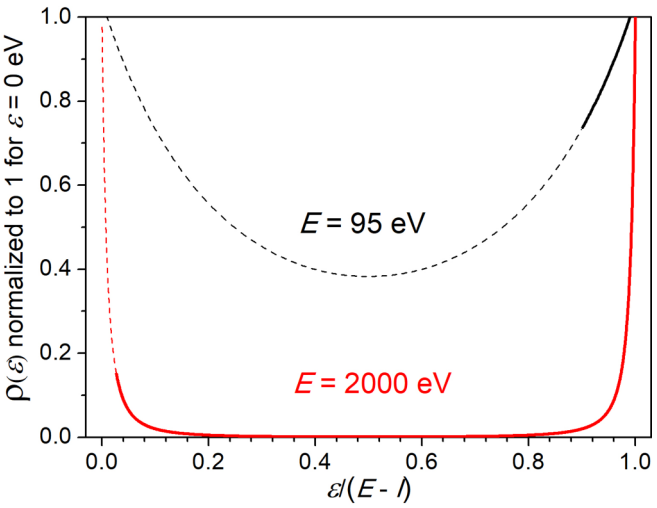

FIG. 3. Energy distribution of the intermediate electron (with kinetic energy ε) in the primary electron-impact single ionization (with ionization potential I) $e^- + O^+(1s^2 2s^2 2p^3\,{}^4S) \rightarrow O^{2+}(1s^2 2s^2 2p^2\,{}^3P) + 2e^-$ for the incident energies $E = 95$ and 2000 eV. The solid lines correspond to the energy range in which the intermediate electron is energetically allowed to knock further out a bound electron of the intermediate O^{2+} ion.

It is found from Fig. 4 that DDI cross sections obtained by the single-configuration approximation are about three times greater than those obtained by the many-configuration approximation for the O^+ ion. This illustrates the importance of the correlation effect in the calculations of the DDI cross sections.

In Fig. 5, we present the DI cross sections of the O^{2+} ion, which are compared with the available theoretical [17] and experimental [9] data. For the present results, the contributions from the direct and indirect processes are also given. The present DI threshold of 130.12 eV agrees with the NIST value [39] of 132.35 eV. It is found that our results are in much better agreement with the experimental measurements [9] compared

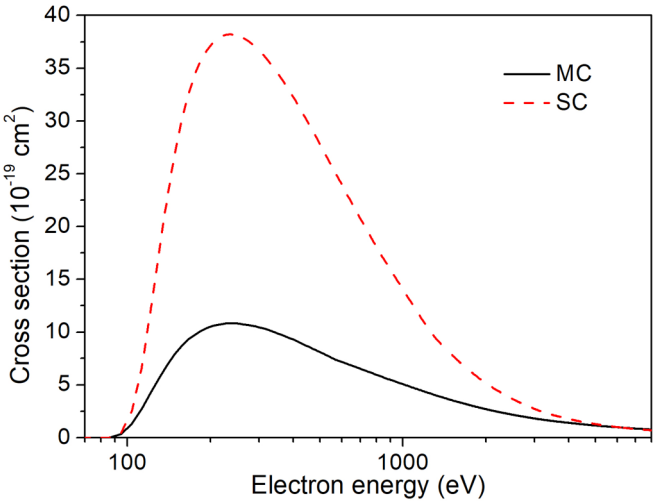

FIG. 4. Electron-impact direct double-ionization cross sections obtained by the single-configuration (SC) and many-configuration (MC) approximations for the O^+ ion.

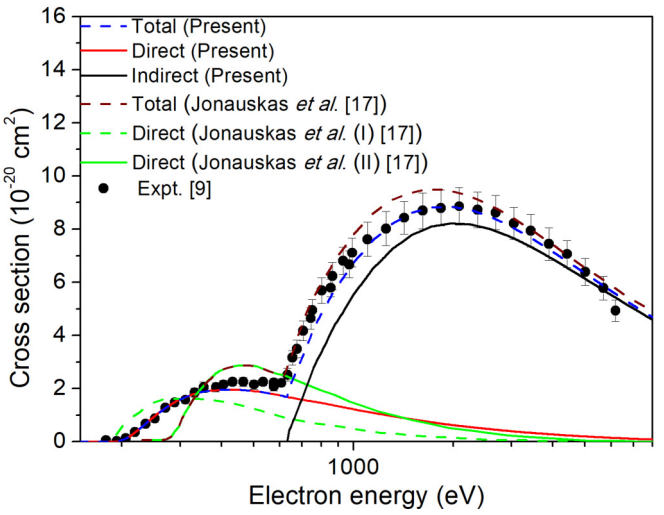

FIG. 6. Theoretical and experimental cross sections for the electron-impact double ionization of the O^{3+} ion. Total: including the cross sections of the direct and indirect processes. Direct: cross section of the direct process. Indirect: cross section of the indirect process.

to the calculations of Jonauskas *et al.* [17] for the energy range considered. Near the ionization threshold, our results are reasonably consistent with those of Jonauskas *et al.* (I), both of which agree with the experimental data [9], while, at the energies above about 200 eV, some significant differences of the magnitude and energy dependence of the DDI cross section between the present calculations and the results of Jonauskas *et al.* (II) are found. For example, our DDI cross sections are greater than the calculations of Jonauskas *et al.* [17] at energies greater than 600 eV. However, the present results show a good agreement with the experimental data, which emphasizes the importance of the intermediate-electron energy distributions once again. We also found that the DI cross sections of the O^{2+} ion show two well-distinguished

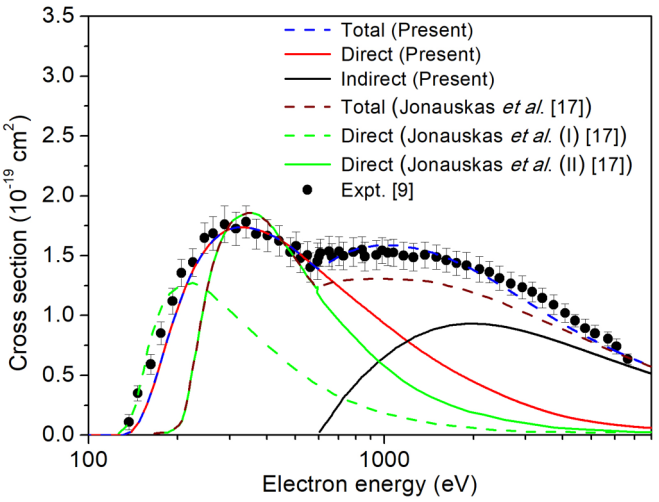

FIG. 5. Theoretical and experimental cross sections for the electron-impact double ionization of the O^{2+} ion. Total: including the cross sections of the direct and indirect processes. Direct: cross section of the direct process. Indirect: cross section of the indirect process.

structures, which are attributed to the contribution from the direct process and the indirect SI-SA process that opens at about 603 eV, respectively. At high energies, the cross sections from the direct process are rather small and they almost result from the indirect process.

Figure 6 exhibits a comparison of our DI cross sections with the calculations of Jonauskas *et al.* [17] and the experimental data [9] for the O^{3+} ion. The present DI threshold of 189.61 eV is in agreement with the NIST value [39] of 191.31 eV. It is also found that the present DI cross sections are in much better agreement with the experimental data than the calculations of Jonauskas *et al.* [17] over a large energy range. For the direct process, the cross sections of Jonauskas *et al.* [17] are greater than ours from the threshold to 1000 eV. For energies greater than 1000 eV, both theoretical results are reasonably consistent with each other. As shown in Fig. 6, our cross sections of the indirect SI-SA channel that starts at about 632 eV become dominant to the total cross section. Meanwhile, the total cross sections of Jonauskas *et al.* [17] are slightly greater than both the present results and experimental [9] data at energies greater than about 700 eV.

For O^+, O^{2+}, and O^{3+} ions, there is a large difference for the DI cross sections between the direct and indirect processes (cf. Figs. 2, 5, and 6). According to our calculations, the maximum of the cross section for the DDI is approximately 10.8×10^{-19}, 1.7×10^{-19}, and 0.2×10^{-19} cm^2 for O^+, O^{2+}, and O^{3+} ions, respectively, while that of the indirect process is determined to be about 1.0×10^{-19}, 0.9×10^{-19}, and 0.8×10^{-19} cm^2. It is found that the maximum of the cross section for the direct process decreases more significantly with increasing the ionization stage than that of the indirect process. The DDI removing two electrons in outer shells simultaneously can be strongly affected by the effective atomic potential due to the screening on the nuclear charge by the bound electrons. This leads to smaller cross sections for removing two bound electrons simultaneously by electron

TABLE I. Single Auger (SA) and double Auger (DA) rates and branching ratios (BR) of the DA process for intermediate states $1s2s^22p^3\,{}^5S$ and ${}^3S$ of the O^{2+} ion. The numbers in brackets represent powers of 10.

	Rate (s^{-1})					
	SA		DA		BR (%)	
Intermediate state	Present	Ref. [36]	Present	Ref. [36]	Present	Ref. [36]
$1s2s^22p^3\,{}^5S$	1.32(14)	1.44(14)	2.56(12)	3.98(12)	1.90	2.70
$1s2s^22p^3\,{}^3S$	8.59(13)	9.22(13)	1.81(12)	2.63(12)	2.06	2.77

impact for the ion with the smaller number of bound electrons (higher ionization stage), while for the indirect process the ionization of the innermost $1s$ electron that sees directly the atomic nucleus can be affected less by the electrons of outer subshells. Thus, with increasing the ionization stage the cross section of the direct process decreases quickly, while that of the indirect process decreases slightly and then becomes dominant like the case of the O^{3+} ion in Fig. 6.

B. Electron-impact triple ionization

To the best of our knowledge, there is no *ab initio* theoretical effort to investigate the TI of the O^+ ion. Here, we propose the approach described in Sec. II B by extending the KO mechanism to deal with the direct process of the TI. Furthermore, we found that the contribution from the indirect process almost results from the primary SI of the inner-shell $1s$ electron to the intermediate autoionizing states O^{2+} ($1s2s^22p^3\,{}^5S$ and ${}^3S$) that undergo the DA decay. It is noted that the direct DA is dominant, while the cascade DA process is negligible in the case of such autoionizing states; moreover, the SA rate is much larger than the radiative decay rate [36]. The total SA and direct DA rates as well as the BRs for these two intermediate states are listed in Table I, which are in agreement with the theoretical results of Zeng *et al.* [36].

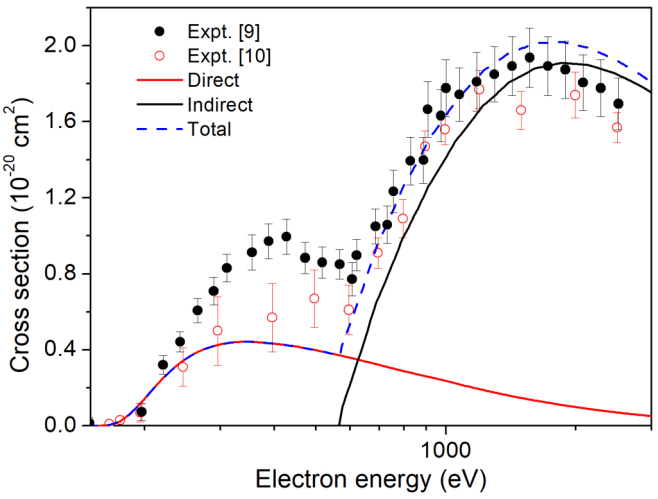

FIG. 7. Theoretical and experimental cross sections for the electron-impact triple ionization of the O^+ ion. Total: including the cross sections of the direct and indirect processes. Direct: cross section of the direct process. Indirect: cross section of the indirect process.

Figure 7 exhibits the calculated TI cross sections of the O^+ ion, along with the experimental data [9,10]. The present TI threshold of 164.71 eV agrees with the NIST value [39] of 167.47 eV and the experimental data [10] of 170 ± 5 eV. In Fig. 7, the earlier experimental values of Westermann *et al.* [9] are greater than the latest ones of Lecointre *et al.* [10] at energies from about 250 to 600 eV (where the cross sections result from the direct process), while they are reasonably consistent with each other at energies greater than 700 eV (where the indirect process dominates). Additionally, for these two experimental measurements there are different energy dependences of the DTI cross section at energies from the threshold to 600 eV.

From Fig. 7, it is found that although the present results are smaller than the earlier experimental values [9] at the energies from the threshold to 600 eV a consistency is shown for the energy dependence of the cross section. Surprisingly, the present TI cross sections agree well with the latest experimental data of Lecointre *et al.* [10], although the slight underestimations (around 500 eV) and overestimations (above 2000 eV) of the calculations are found. Such differences possibly originate from (a) the simplified energy distribution of intermediate electrons (three outgoing continuum electrons in the primary DDI), (b) the limited intermediate states due to computational resources, and (c) the absences of other radiative and radiationless stabilizations such as triple Auger decay in the calculations of the BR in Eq. (13) at high energies. These issues should be addressed in future works, and further experiments are expected.

IV. CONCLUSIONS

In this paper, theoretical investigations of the DI of O^+, O^{2+} and O^{3+} ions as well as the TI of the O^+ ion are performed in the framework of MBPT. Two competing channels of the direct and indirect ionization processes are considered independently. The IDI and ITI are described as a two-step process in which the primary single ionization of the inner-shell $1s$ electron is followed by the SA and DA decays, respectively. The DDI and DTI are decomposed into the primary ionization and the subsequent KO (electron-electron inelastic scattering). Furthermore, the normalized DCS of the primary ionization is considered as the energy distribution of the intermediate electrons that participate in the subsequent KO process. According to the corresponding approximate

formulas, we calculate the DI cross sections of the O^+, O^{2+}, and O^{3+} ions using the FAC package with DW approximation, which are in excellent agreement with the available experimental data. Moreover, the *ab initio* studies of the TI are presented for the O^+ ion and the cross sections are calculated, which agree well with the recent experimental measurements [10]. The present paper indicates that the multistep approaches based on the KO mechanism can describe properly the direct MI of O^+, O^{2+}, and O^{3+} ions and, more importantly, elucidate the significant role of the electron correlation and the energy distribution of the intermediate electron in describing multiple ionization processes.

ACKNOWLEDGMENTS

This work was supported by the National Key Research and Development Program of China (Grant No. 2017YFA0402300), the National Natural Science Foundation of China (Grants No. 11934004, No. 11774037, and No. U1530142), and the China Postdoctoral Science Foundation (Grant No. 2019M650582).

[1] J. Berakdar, A. Lahmam-Bennani, and C. Dal Cappello, Phys. Rep. **374**, 91 (2003).
[2] A. Lahmam-Bennani, I. Taouil, A. Duguet, M. Lecas, L. Avaldi, and J. Berakdar, Phys. Rev. A **59**, 3548 (1999).
[3] M. Hahn and D. W. Savin, Astrophys. J. **800**, 68 (2015).
[4] M. Hahn and D. W. Savin, Astrophys. J. **809**, 178 (2015).
[5] V. P. Shevelko, H. Tawara, I. Yu. Tolstikhina, F. Scheuermann, B. Fabian, A. Müller, and E. Salzborn, J. Phys. B **39**, 1499 (2006).
[6] M. Hahn, A. Müller, and D. W. Savin, Astrophys. J. **850**, 122 (2017).
[7] V. P. Shevelko, H. Tawara, F. Scheuermann, B. Fabian, A. Müller, and E. Salzborn, J. Phys. B **38**, 525 (2005).
[8] M. Zambra, D. Belic, P. Defrance, and D. J. Yu, J. Phys. B **27**, 2383 (1994).
[9] M. Westermann, F. Scheuermann, K. Aichele, U. Hartenfeller, D. Hathiramani, M. Steidl, and E. Salzborn, Phys. Scr. **T80**, 285 (1999).
[10] J. Lecointre, K. A. Kouzakov, D. S. Belic, P. Defrance, Y. V. Popov, and V. P. Shevelko, J. Phys. B **46**, 205201 (2013).
[11] M. S. Pindzola, F. J. Robicheaux, J. P. Colgan, M. C. Witthoeft, and J. A. Ludlow, Phys. Rev. A **70**, 032705 (2004).
[12] M. S. Pindzola, F. Robicheaux, S. D. Loch, J. C. Berengut, T. Topcu, J. Colgan, M. Foster, D. C. Griffin, C. P. Ballance, D. R. Schultz, T. Minami, N. R. Badnell, M. C. Witthoeft, D. R. Plante, D. M. Mitnik, J. A. Ludlow, and U. Kleiman, J. Phys. B **40**, R39 (2007).
[13] J. Colgan and M. S. Pindzola, Eur. Phys. J. D **66**, 284 (2012).
[14] A. Müller, Adv. At. Mol. Opt. Phys. **55**, 293 (2008).
[15] M. H. Mittleman, Phys. Rev. Lett. **16**, 498 (1966).
[16] M. Gryziński, Phys. Rev. **138**, A336 (1965).
[17] V. Jonauskas, A. Prancikevičius, Š. Masys, and A. Kynienė, Phys. Rev. A **89**, 052714 (2014).
[18] J. Koncevičiūtė and V. Jonauskas, Phys. Rev. A **93**, 022711 (2016).
[19] J. Koncevičiūtė, S. Kučas, Š. Masys, A. Kynienė, and V. Jonauskas, Phys. Rev. A **97**, 012705 (2018).
[20] J. Koncevičiūtė, S. Kučas, A. Kynienė, Š. Masys, and V. Jonauskas, J. Phys. B **52**, 025203 (2018).
[21] T. Schneider, P. L. Chocian, and J.-M. Rost, Phys. Rev. Lett. **89**, 073002 (2002).
[22] T. Schneider and J.-M. Rost, Phys. Rev. A **67**, 062704 (2003).
[23] E. P. Månsson, D. Guénot, C. L. Arnold, D. Kroon, S. Kasper, J. M. Dahlström, E. Lindroth, A. S. Kheifets, A. L'Huillier, S. L. Sorensen, and M. Gisselbrecht, Nat. Phys. **10**, 207 (2014).
[24] M. Y. Amusia, I. S. Lee, and V. A. Kilin, Phys. Rev. A **45**, 4576 (1992).
[25] J. Zeng, P. Liu, W. Xiang, and J. Yuan, Phys. Rev. A **87**, 033419 (2013).
[26] F. Zhou, Y. Ma, and Y. Qu, Phys. Rev. A **93**, 060501(R) (2016).
[27] Y. Ma, F. Zhou, L. Liu, and Y. Qu, Phys. Rev. A **96**, 042504 (2017).
[28] Y. Ma, Z. Liu, F. Zhou, and Y. Qu, Phys. Rev. A **98**, 043417 (2018).
[29] Y.-L. Ma, F.-Y. Zhou, Z.-Q. Liu, and Y.-Z. Qu, Chin. Phys. B **27**, 063201 (2018).
[30] J. A. Tanis, J. Y. Chesnel, F. Frémont, D. Hennecart, X. Husson, A. Cassimi, J. P. Grandin, B. Skogvall, B. Sulik, J. H. Bremer, and N. Stolterfoht, Phys. Rev. Lett. **83**, 1131 (1999).
[31] J. A. Tanis, J.-Y. Chesnel, F. Frémont, D. Hennecart, X. Husson, D. Lecler, A. Cassimi, J. P. Grandin, J. Rangama, B. Skogvall, B. Sulik, J.-H. Bremer, and N. Stolterfoht, Phys. Rev. A **62**, 032715 (2000).
[32] P. Liu, J. Zeng, and J. Yuan, J. Phys. B **51**, 075202 (2018).
[33] M. F. Gu, Can. J. Phys. **86**, 675 (2008).
[34] J. H. McGuire, Phys. Rev. Lett. **49**, 1153 (1982).
[35] Y.-K. Kim and M. E. Rudd, Phys. Rev. A **50**, 3954 (1994).
[36] J. Zeng, Y. Li, P. Liu, C. Gao, and J. Yuan, Astron. Astrophys. **605**, A32 (2017).
[37] C. Dal Cappello, R. El Mkhanter, and P. A. Hervieux, Phys. Rev. A **57**, R693 (1998).
[38] A. Duguet, C. Dupré, and A. Lahmam-Bennani, J. Phys. B **24**, 675 (1991).
[39] A. Kramida, Yu. Ralchenko, J. Reader, and NIST ASD Team, NIST Atomic Spectra Database (ver. 5.7.1), https://physics.nist.gov/asd (2019).
[40] P. Defrance, J. J. Jureta, T. Kereselidze, J. Lecointre, and Z. S. Machavariani, J. Phys. B **42**, 025202 (2008).